Etching mechanism of diamond by Ni nanoparticles for fabrication of nanopores

Hasan-Al Mehedi, Jean-Charles Arnault, David Eon, Clément Hébert, Davy Carole, Franck Omnès, Etienne Gheeraert

Etching mechanism of diamond by Ni nanoparticles for fabrication of nanopores

Hasan Al Mehedi (a), Jean-Charles Arnault (b), David Eon (a), Clément Hébert (a), Davy Carole (c), Franck Omnes (a), Etienne Gheeraert (a)

(a) Institut Néel, CNRS et Université Joseph Fourier, BP 166, F-38042 Grenoble Cedex 9, France

(b) Diamond Sensors Laboratory, CEA/LIST, Centre d'Etudes de Saclay, F-91191 Gif Sur Yvette, France

(c) LMI, CNRS and Université Claude Bernard Lyon 1, 43 Bd du 11 november 1918, F-69622 Villeurbanne Cedex, France

Abstract

Nanopores in insulating solid state membranes have recently emerged as potential candidates for sorting, probing and manipulating biopolymers, such as DNA, RNA and proteins in their native environment. Here a simple, fast and cost-effective etching technique to create nanopores in diamond membrane by self-assembled Ni nanoparticles is proposed. In this process, a diamond film is annealed with thin Ni layers at 800–850 °C in hydrogen atmosphere. Carbon from the diamond–metal interface is removed as methane by the help of Ni nanoparticles as catalyst and consequently, the nanoparticles enter the crystal volume. In order to optimize the etching process and understand the mechanism the annealed polycrystalline and nanocrystalline diamond films were analyzed by X-ray photoelectron spectroscopy (XPS), and the gas composition during the process was investigated by quadrupole mass spectrometer. With this technique, nanopores with lateral size in the range of 15–225 nm and as deep as about 550 nm in diamond membrane were produced without any need for lithography process. A model for etching diamond with Ni explaining the mechanism is discussed.

1. Introduction

Like their biological counterparts [1], artificially engineered nanopores in solid-state membranes constitute versatile and robust devices to investigate molecular properties of biomolecules [2] and biomolecular interactions [3]. The nanopore sensing concept utilizes chips (typically made in silicon (Si)) that contain a thin free-standing membrane into which a nanometer-sized hole (nanopore) is drilled [2], [4]. When a nanopore chip is immersed in a conducting electrolyte solution containing analyte molecules and an electric field is applied across the membrane, the molecules could partially block the ionic current upon passage through the pore [5]. Individual molecule could then be detected by measuring the time duration and magnitude of current blockage. Notable examples include nanopores in SiO_2 and Si_3N_4 membranes fabricated by using either an Ar^+ beam [5], [6] or an electron beam (e-beam) in a transmission electron microscope [7], [8].

Such nanopore sensing systems offer high stability against pressure variations and mechanical vibrations and thus give more reproducible results. However, analyzing molecules in harsh conditions such as extreme temperatures, voltages or pH conditions could lead to the malfunctioning or in extreme cases to the destruction of the

chips with conventional membranes. The problem can be solved by establishing nanopores in diamond since this material possesses exceptional physio-chemical properties such as the highest hardness and Young's modulus (1200 GPa) of all known solids, a very high thermal conductivity (20–22 W cm^{-1} K^{-1}) and a low thermal expansion coefficient [9], [10], [11], [12]. Furthermore, because of its wide band gap, the electrochemical potential window of diamond is significantly larger and the background current within this regime considerably lower than conventional electrodes made from metals or graphite [13]. This behavior enables detection with low noise over a wide potential range.

Since diamond is chemically inert in gases and liquids at room temperature, the etching of diamond required for the device fabrication is performed almost exclusively by the reactive ion etching (RIE) technique with the help of lithographical processes, lithography being used for mask deposition [14], [15], [16]. However, with the RIE, fabrication of very narrow (10–50 nm in lateral size) and long (typically longer than 300 nm) pores has become problematic due to the limitation in lithographic resolution and high aspect ratio etching profiles. In addition, an unavoidable use of the e-beam lithography for fabricating high resolution nanostructures makes the RIE process costly and time consuming.

We have previously reported on the metal catalyst-assisted etching of polycrystalline and nanocrystalline diamond in hydrogen atmosphere for nanopore generation in the diamond membrane [17]. The role of different process parameters such as metal type, process temperature and time, hydrogen pressure, and diamond microstructure was investigated extensively. However, the etching mechanism was not fully understood. In this article, we extended our investigation to get further insight into the etching process and thereby to develop a model explaining the mechanism. For this purpose, we emphasized the influence of etching time, nanoparticle size and annealing atmosphere in the etching process and measured the chemical composition of the gas during etching. Surface chemistry of the samples was analyzed by XPS, while their morphology was examined using scanning electron microscopy (SEM). Ni was used as a potential catalyst since it showed the highest etching activity among the studied metals (Co, Pt and Au) [17].

The etching mechanism was investigated based on the reported works that dealt with catalytic formation of nano-holes and nano-channels (open tube) in the surface layers of highly oriented pyrolytic graphite and diamond [18], [19], and patterning of diamond surfaces [20]. The etching of diamond was suggested to be accompanied with the formation of a carbide-like layer containing hydrogen at the diamond–metal interface and the successive formation of this layer was thought to assist the moving of nanoparticles resulting in the channeling of diamonds [19]. In contrast, Ralchenko et al. [20] interpreted the etching according to a mechanism involving carbon dissolution in metal, followed by diffusion from the diamond–metal to the metal–gas interface and finally desorption of carbon as hydrocarbons.

2. Experimental

2.1. Etching of diamond films

The etching technique consists of two steps, (i) the deposition of thin Ni layers on a diamond substrate, and (ii) the subsequent annealing of the substrate in hydrogen atmosphere. The Ni layer with thickness in the range of 1–15 nm was deposited by e-beam evaporation, the thickness being measured by a quartz oscillator. The annealing step was carried out in a chemical vapor deposition (CVD) reactor, usually dedicated to diamond growth, at 800–850 °C in 60 Torr flowing hydrogen with 100 standard cubic centimeter per minute (sccm, at STP). The base pressure of the reactor before the process was $<10^{-6}$ Torr. The temperature was increased from room temperature at a rate of ~200 °C/min and measured with an infrared pyrometer with a reading precision of ±10 °C. After the annealing step, the samples were cooled down for 30 min under continuous hydrogen flow.

Two types of diamond films were used for these experiments, namely polycrystalline diamond with grain size of typically 50 μm (Fig. 1a) and nanocrystalline diamond (grain size 100 nm) (Fig. 1b). Polycrystalline diamond was obtained from Element Six (electrochemical grade boron doped CVD diamond). Nanocrystalline diamond (undoped) with a thickness of about 1.5 μm was grown on a silicon substrate in a microwave plasma CVD reactor (Seki-ASTEX 5200 MPCVD system) using the bias enhanced nucleation method [21] with following parameters: 900 °C temperature, 1000 W microwave power, 0.3% methane in hydrogen, and pressure of 30 Torr.

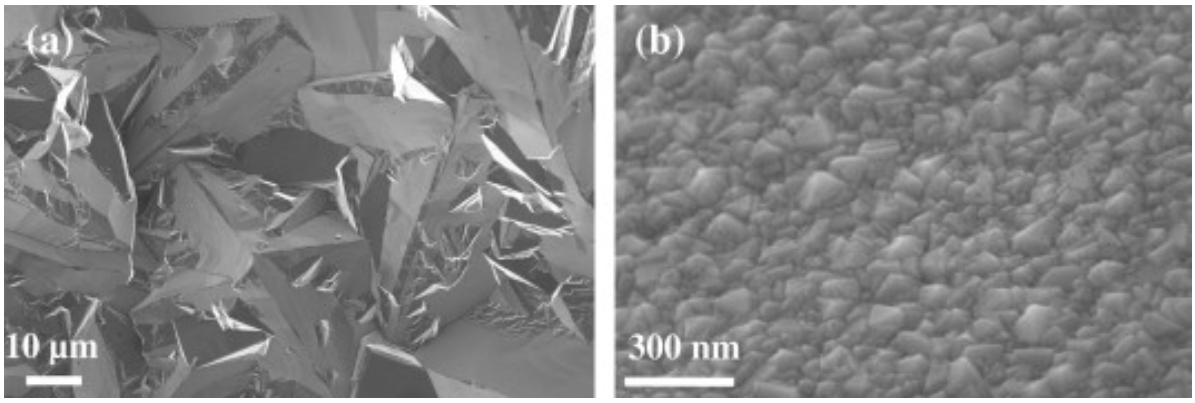

Fig. 1. SEM images of **(a)** as-received polycrystalline diamond and **(b)** nanocrystalline diamond with average grain size of about 50 μm and 100 nm, respectively. Polycrystalline diamond substrates are electrochemical grade boron doped CVD diamond purchased from element six, whereas nanocrystalline diamond films are grown on Si substrates in a MPCVD reactor using bias enhanced nucleation approach.

2.2. Analysis of the chamber gas with mass spectrometer

A quadrupole mass spectrometer gas analyzer (AMETEK Dycor Dymnaxion DM 100) was fitted to the exhaust port of the reaction chamber with an aperture inlet consisting of a 5 μm aperture within a manual valve. The aperture was chosen to reduce the pressure from 60 Torr in the process chamber down to 10^{-5} Torr in the quadrupole. The detection set consisted of a Faraday cup detector, and an electron multiplier was used to amplify the signal by approximately one thousand. The minimum detectable partial pressure for the Faraday cup detector is 5×10^{-12} Torr and that for electron multiplier units is 5×10^{-14} Torr with mass resolution of 0.5 AMU at 10% height.

2.3. XPS measurement

The XPS measurements were performed on the samples after process, with a monochromatic Al Kα anode (1486.6 eV) that was calibrated with respect to the Au $4f_{7/2}$ peak located at 84.0 eV. The spectrometer was equipped with an EA 125 hemispherical analyzer. The path energy was 20 eV corresponding to an absolute energy resolution of 0.6 eV. The detection limit of our XPS setup is estimated to be 0.2 at.%. Areas of XPS core levels were extracted after a Shirley correction of the background and atomic contents were calculated after correction by the photoionized cross-sections. For the XPS measurement, the detection of any component is strongly influenced by the penetration depth of X-ray (probed depth d) that is calculated by:

$$(1)\ d=3\lambda\cos\theta$$

where λ is the mean free path of photoelectrons and θ is the angle between the surface normal and the analyzer direction (for our XPS geometry, $\theta = 41°$). According to our experimental conditions, probed depths for C 1s and Ni 2p were estimated to be 7.0 and 2.3 nm taking into account λ values of 3.1 and 1.0 nm respectively [22].

3. Results and discussion

3.1. Formation of nanopores into diamond films

For this study, samples were processed in the temperature range 800–850 °C as no sign of etching was observed below 800 °C in 60 Torr hydrogen with increasing thickness of evaporated Ni film [17]. Fig. 2 shows SEM images of (1 0 0) surface of annealed polycrystalline diamond in the case of 3 nm Ni layers.

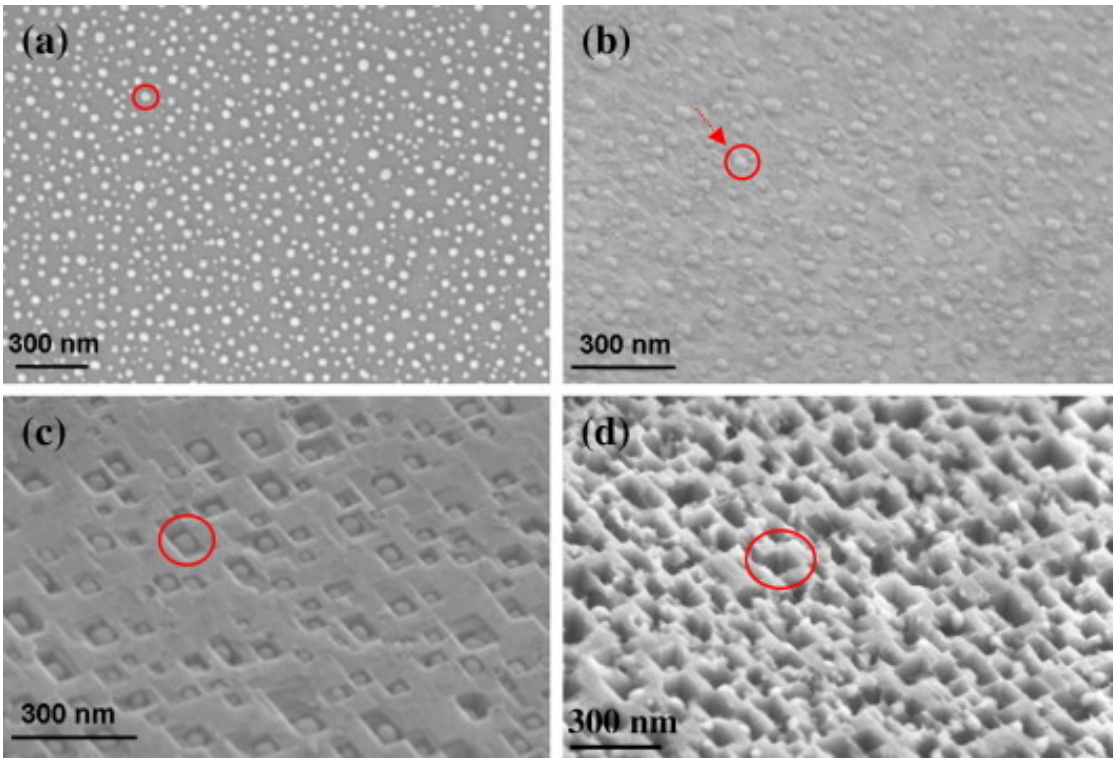

Fig. 2. SEM images of (1 0 0) surface of annealed polycrystalline diamond after **(a)** 30 s, **(b)** 3 min, **(c)** 10 min and **(d)** 6 h of annealing with 3 nm Ni layers, (800 °C, 60 Torr H_2). The red circle identifies a particular particle evolution, and the red arrow indicates the movement of the particle due to gravity prior to etching. (For interpretation of the references to colour in this figure legend, the reader is referred to the web version of this article.)

After 30 s of annealing at 800 °C we observed self-organized Ni nanoparticles on the surface (Fig. 2a). Etched structures started to appear after 3 min (Fig. 2b), and nanopores with flat sidewall faces and sharply defined edges were formed after 10 min of annealing (Fig. 2c). 6 h annealing resulted in nanopores with ruptured edges and sidewall faces (Fig. 2d). In addition, while not conclusive, movement of the particle due to gravity was observed prior to etching.

During annealing the Ni layer melts and forms spherically shaped nanoparticles prior to etching in order to minimize the surface energy. This effect is well known and relates to the melting point lowering effect of thin metal films and hydrogen diffusion into the metal [23], [24], [25]. The solid Ni droplets, as seen in Fig. 2c on (1 0 0) diamond surface, are of round shape, while the pits in which they seat are rectangular. We can expect that at high temperature the droplets are liquid, and the contact surface between nickel and diamond is very large. However, because of the high surface energy, the droplet cannot wet completely the pit bottom or corners. Also, the etch pattern is usually much larger than the droplet indicating that etching occurs even if there is no contact between nickel and diamond. This observation suggests an important contribution of atomic surface diffusion in the process.

We estimated the diameter of the resulting nanoparticles to be approximately ten times larger than the initially evaporated Ni layer thickness. Fig. 2c suggests that the size of the nanopores depends on the size of the initially formed Ni nanoparticles and can be adjusted to a certain

extent by the Ni layer thickness, as is shown in Fig. 3a which shows the diameter distribution of nanopores with the Ni layer thickness. Nanopore diameter was estimated by the analysis of the SEM images. Diameter was considered for the pore size since most of the nanopores had a circular section in first approximation in the case of nanocrystalline diamond. The mean diameter of the nanopores was observed to increase with the Ni layer thickness (Fig. 3a). We also calculated the ratio of the mean diameter of the nanopores to that of Ni particles to be approximately 1.5:1. In contrast to the diameter distribution, the density of the nanopores was found to decrease with the Ni layer thickness (Fig. 3a). During annealing small Ni particles generated initially from relatively thick film, e.g. 15 nm Ni layers, could coalescence /and dissolve into the big particles through surface migration and growth that could result in the decrease of the density of active Ni particles for etching. The SEM image of Fig. 3b shows the largest nanopores with mean lateral size of about 225 nm that were achieved by annealing the nanocrystalline diamond at 850 °C with 15 nm Ni layers for 10 min, whereas the smallest nanopores with mean size of about 15 nm were obtained in the case of 1 nm Ni layer (Fig. 3c).

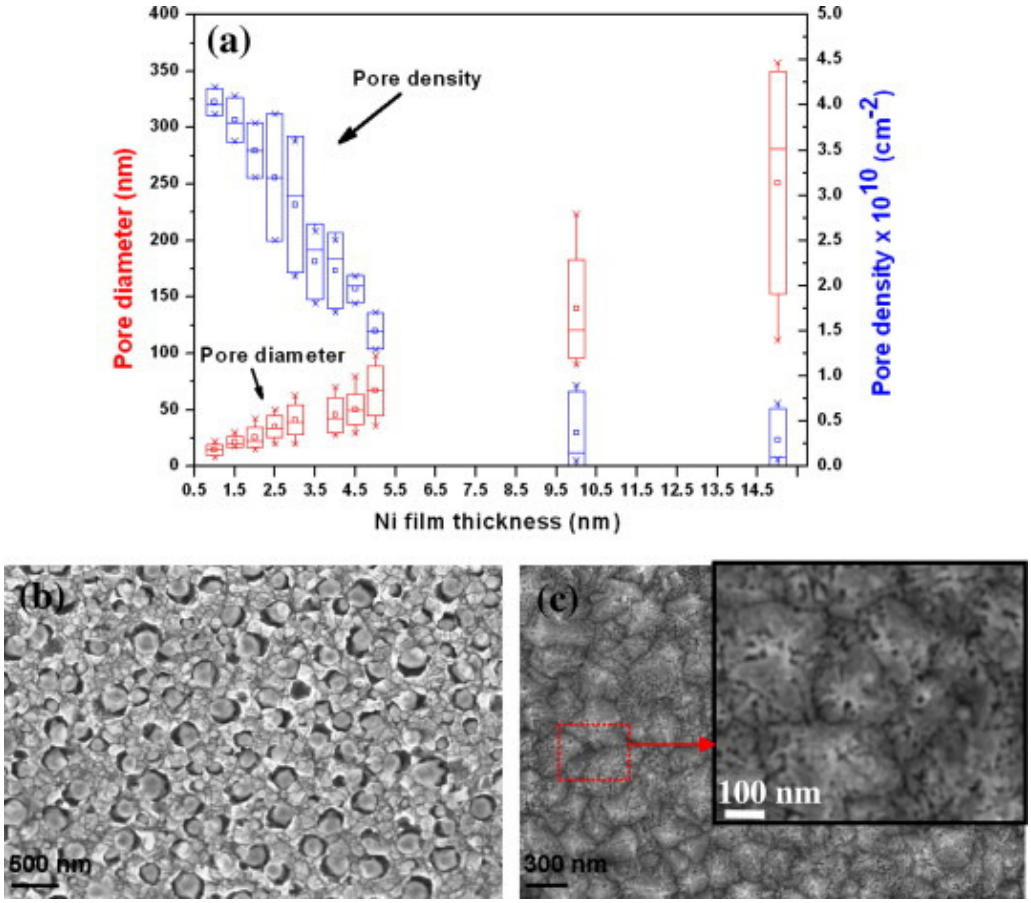

Fig. 3. (a) Nanopore diameter and density distribution measured for nanocrystalline diamond after 10 min annealing with Ni layers of thickness of 1–15 nm, (850 °C, 60 Torr H_2). The box represents standard deviation. The band and square inside refer to median and mean respectively; minimum and maximum values are indicated by the cross. Nanopore diameter and density were estimated by analyzing the SEM images of each processed sample. **(b)** Corresponding SEM image showing the largest pores with mean diameter of 225 nm produced by Ni particles generated from 15 nm Ni layers, whereas **(c)** showing the smallest pores (~15 nm) obtained in the case of 1 nm Ni layer; the inset is a magnified image of the marked section.

Nanocrystalline diamond samples exhibit a mixture of [1 1 1] and [1 0 0] oriented planes, and the etching behavior is different depending on the crystallographic orientation. While pyramidal shaped nanopores were formed on the (1 0 0) surface of diamond, a mixture of pyramidal, conical and cylindrical shaped nanopores were found on the nanocrystalline diamond. Such orientation dependence of diamond etching has been investigated extensively by using molten Ce [26], Fe particles [27], Co nanoparticles [28], and molten Ni [29], as catalysts. It has been shown that Ni assisted diamond etching is slowest for [1 1 1] oriented diamond planes and that they act as stopping planes [29]. Since the uptake of carbon atoms from diamond by the metal nanoparticles occurs preferentially from the weakly bonded atoms, the carbon atoms of the closest packing plane, {1 1 1} planes, are the most stable against the dissolution of carbon in nanoparticles, as compared to the other crystal planes [29]. As a result, nanopores walled with four {1 1 1} planes are formed on the {1 0 0} surfaces whereas {1 1 1} show pores with equilateral triangles and hexagons [28], [29]. The effect of deposited Ni thickness on nanopore depth was then studied. The results are plotted in Fig. 4a.

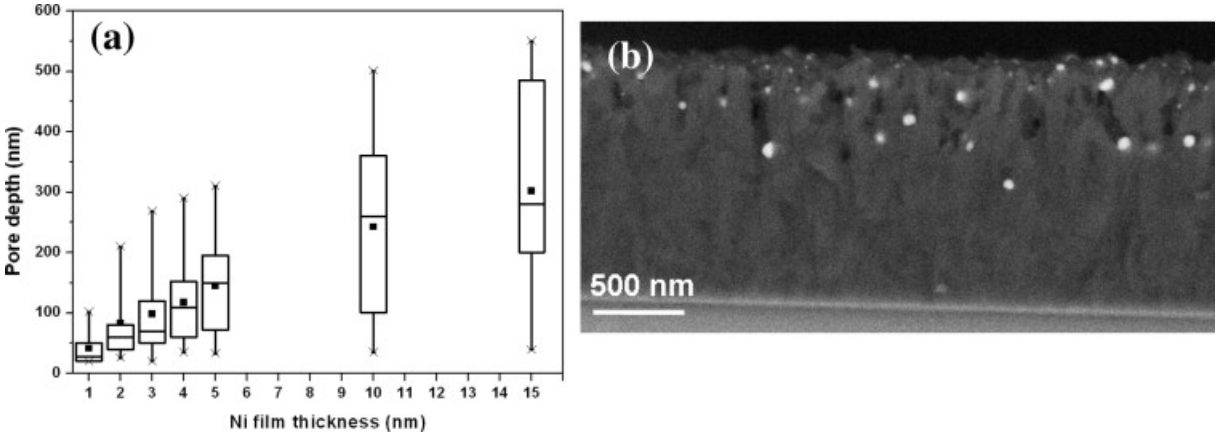

Fig. 4. (a) Nanopore depth distribution measured for nanocrystalline diamond after 10 min annealing with Ni layers of thickness of 1–15 nm (850 °C, 60 Torr H_2). After annealing, cross-sections of each processed sample were observed by SEM and pore depth was estimated by analyzing the images. Bottom and top line of the box represents 25th and 75th percentile of each data set respectively. The band and square inside refer to median and mean respectively; minimum and maximum values are indicated by the cross. Whiskers refer to standard deviation ± mean. **(b)** SEM image, acquired with a backscattered electron detector, of the cross-section of an etched nanocrystalline diamond after 60 min annealing with 3 nm Ni layers; bright spots correspond to Ni nanoparticles.

Nanocrystalline diamond was annealed with Ni layers of thickness of 1–15 nm for 10 min at 850 °C. The depth of nanopores was measured by SEM on cross sections of each processed sample, as is shown in Fig. 4b for 3 nm Ni. The bright contrast corresponds to Ni nanoparticles that were embedded into the diamond crystal. From this investigation we observed the increase in nanopore depth with the Ni layer thickness, in particular, for 10 and 15 nm Ni layers. As the carbon atoms etched from the diamond surface have to diffuse through the catalyst particle to reach the gas phase, this increase in depth shows that the etching of diamond is not limited by the diffusion of carbon through the particle. The limitation factor could therefore be the processes occurring at the catalyst–diamond interface, in particular the formation of carbide, or in the gas phase.

Hydrogen is necessary in the etching process since no etching was observed when the polycrystalline diamond was annealed in vacuum [17]. Moreover, the higher the pressure of hydrogen gas in the chamber, the faster the diamond was etched [17]. The role of hydrogen is however not completely clear. We assumed that hydrogen could be dissociated catalytically into atomic hydrogen by Ni nanoparticles and gasify the dissolved carbon within the particles and the amorphous carbon that could appear at the surface of the catalyst to form methane or some CH_x complex. High hydrogen pressure could enhance the desorption process of carbon and thereby accelerate the etching of diamond.

3.2. Analysis of annealed diamond surfaces by XPS

In order to explore the existence of nickel carbide at the catalyst–diamond interface that could limit the etching process, we investigated the surface composition of annealed samples by XPS. Two polycrystalline diamond films with 3 nm Ni layers were annealed for 30 s and 10 min at 800 °C in 60 Torr hydrogen atmosphere. The corresponding SEM images are displayed in Fig. 2a and c. The samples were then characterized by XPS. The XPS spectra of C 1s and Ni 2p core levels are shown in Fig. 5.

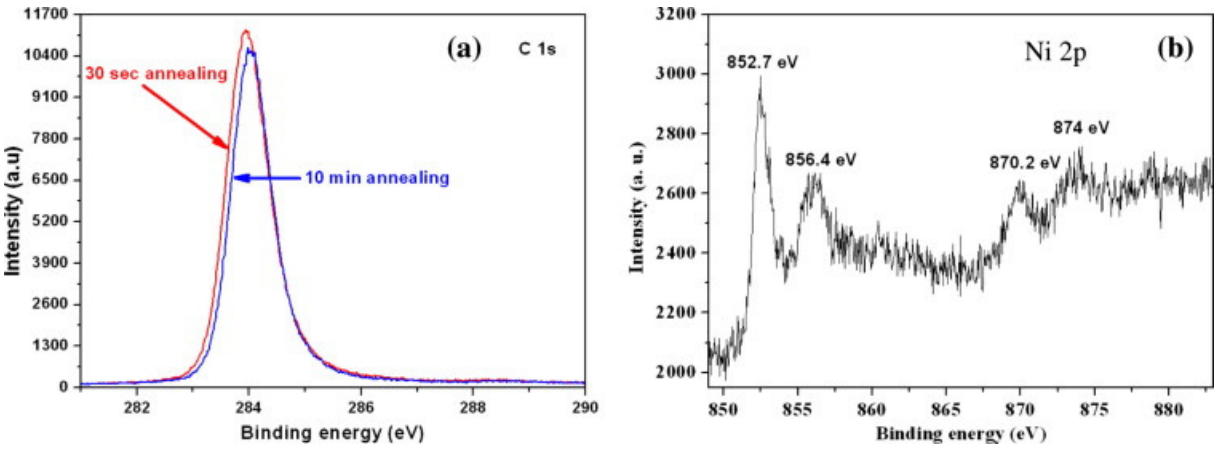

Fig. 5. XPS spectra of **(a)** C 1s core level for 30 s and 10 min annealed polycrystalline diamond with 3 nm Ni layers showing similar peak at 284 eV, that is related to the sp hybridized carbon atoms at the diamond surface, and **(b)** Ni 2p core level for 10 min annealed polycrystalline diamond showing the signature of metallic Ni at 852.7 eV (Ni 2p3/2) and oxide (Ni_2O_3) at 856.4 eV.

The C 1s spectra for 30 s and 10 min annealed diamond films show similar carbon peak at 284 eV (Fig. 5a) that is related to the sp^3 hybridized carbon atoms of diamond surface [30]. Ni 2p core level spectrum (Fig. 5b) obtained from 10 min annealed diamond shows the signature of metallic nickel at 852.7 eV (Ni 2p3/2) and nickel oxide (Ni_20_3) at 856.4 eV [31]. Similar spectrum was obtained for 30 s annealed diamond. For both samples, the spectra of C 1s and Ni 2p core levels did not show carbide component. According to the literature, metallic carbides lead to the presence of an additional component at C 1s located at lower binding energy (~283 eV) vs diamond one [32], [33]. On the other hand, energy loss spectra (ELS, Fig. 6) recorded at C 1s core level for 30 s and 10 min annealed diamond exhibit the characteristic diamond bulk plasmon at +34 eV and surface plasmon at +24 eV from the C 1s [34].

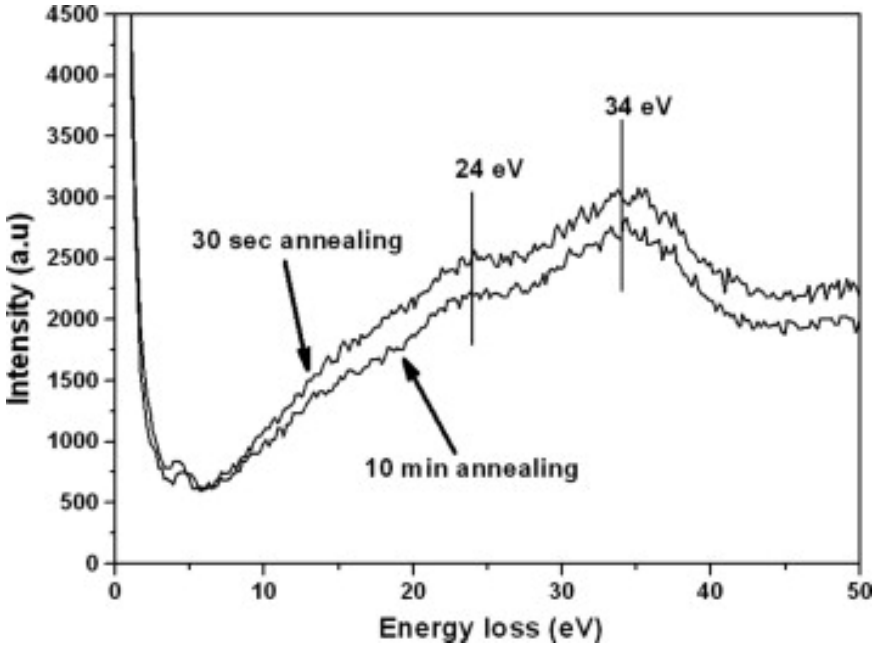

Fig. 6. ELS spectra recorded at the C 1s core level for 30 s and 10 min annealed polycrystalline diamond with 3 nm Ni layers showing the characteristic diamond bulk plasmon at +34 eV and surface plasmon at +24 eV and suggesting no change in the diamond structure after catalytic etching by Ni nanoparticles.

The result suggests that the diamond structure was maintained after the catalytic etching by Ni nanoparticles. Probed depths for C 1s and Ni 2p were estimated to be 7.0 and 2.3 nm taking into account λ values of 3.1 and 1.0 nm, respectively [22]. On the other hand, the diameter of the spherically shaped Ni nanoparticles generated from the 3 nm Ni layers was estimated to be approximately 45 nm. Any component, e.g. carbide, that might form at the diamond–metal interface or present within the particles below the probed depth was therefore not detectable. We also investigated the interface by XPS after removing Ni particles from the 10 min annealed diamond by aqua regia (HCl/HNO_3 3:1). The spectrum (not shown) again did not show any carbide component. No carbide was therefore detected before or after the removal of the nickel catalyst. However, we cannot completely exclude the occurrence of carbide at the interface during the process at 800 °C. There could be a thin layer of carbide at the interface hidden by the Ni nanoparticles, but was etched away together with the nanoparticles by aqua regia.

3.3. Gas composition analysis

For the better understanding of the etching process, the gas composition in the chamber was analyzed during the process. Starting from pure hydrogen, the atmosphere was progressively contaminated by carbon species coming out of diamond. In order to increase the signal, the process was carried out in closed chamber (no hydrogen flow) and a 2 inch nanocrystalline diamond was used. Temperature was 800 °C and 3 nm Ni layers were deposited on the sample. After 1 min of process, methane was detected by the spectrometer (Fig. 7b). The process was carried on for 6 h. Fig. 7c shows the evolution of the total number of carbon atoms in the gas phase. Two different regimes were observed: rapid etching within first 60 min, then slow etching and eventually saturation after about 90 min. In order to compare these results with the SEM observations, the number of carbon atoms removed from the diamond surface

during etching was estimated from the average diameter and depth of the nanopores and shown as dotted line in Fig. 7c.

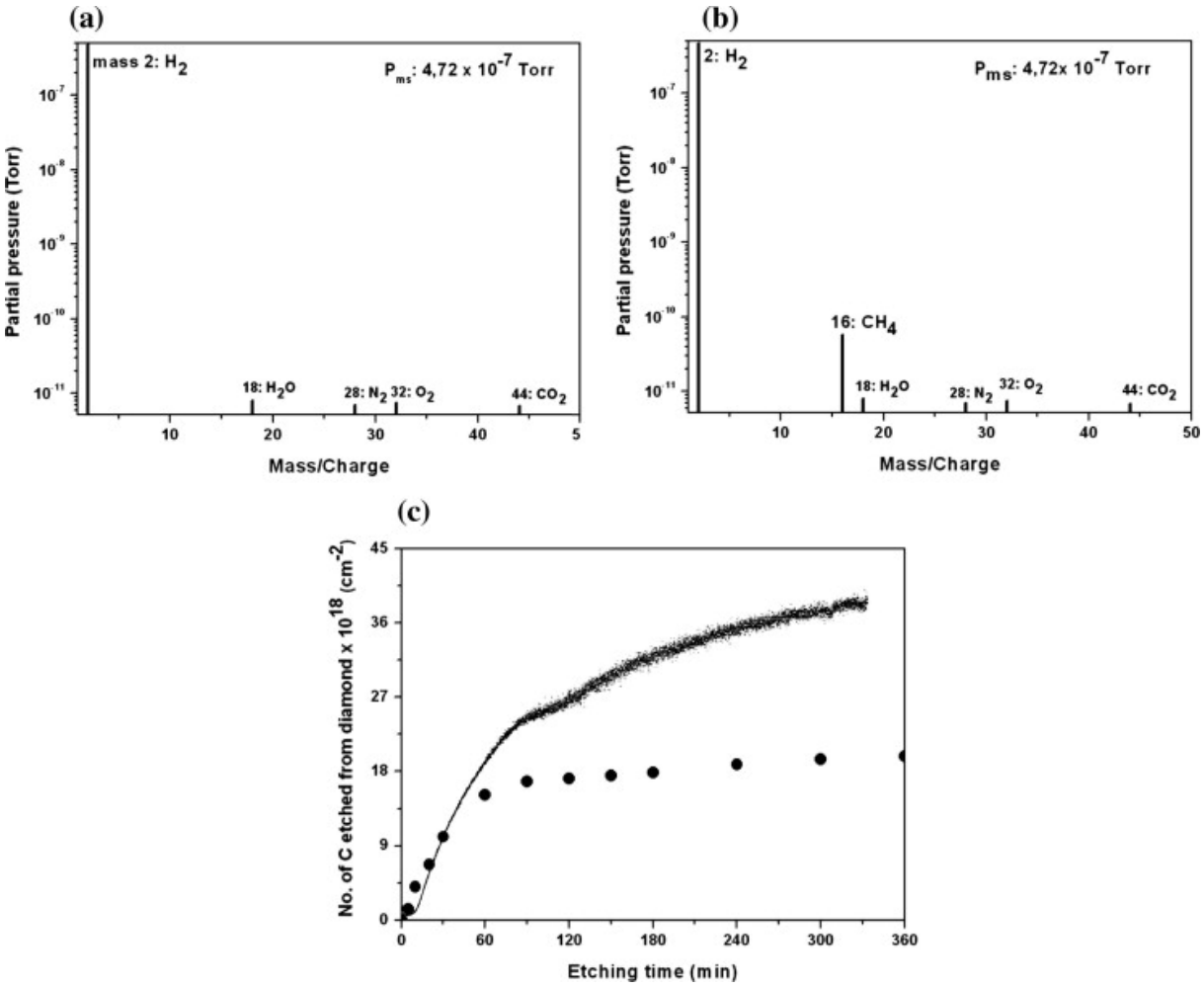

Fig. 7. Mass spectra **(a)** before annealing, hydrogen being added in the gas phase, **(b)** after 1 min of the process revealing the release of carbon atoms from the diamond, and **(c)** number of carbon atoms removed from nanocrystalline diamond during 6 h of the process (800 °C, 3 nm Ni, 60 Torr H_2). In panel **(c)**, solid line represents spectrometer data, whereas the dotted line corresponds to the number of removed carbon atoms calculated from the average depth and diameter of the nanopores. P_{ms} indicates pressure in the spectrometer head.

The agreement is quite convincing, confirming that the methane is coming out of the nanopores, and that methane is the main hydrocarbon species carrying etched carbon atoms. The observed behavior of methane evolution could explain the etching process in the following ways:

- For short etching time (before typically 60 min of etching); the process is limited by the kinetics at the catalyst–diamond interface and the etching rate is roughly constant.
- For long etching time (between 60 and 90 min); the catalyst droplets are already located deep inside the diamond film (300–500 nm) resulting in the reduction of both the diffusion of hydrogen into the pores and the out-diffusion of methane from the pores. Thereby, the carbon desorption from the nickel catalyst is decreased. If the desorption rate is not high enough to remove all the carbon, a graphite-like film can be formed at

outer metal surface causing catalyst deactivation [35]. Those areas which turn out to be covered by carbon films show a slower etch rate.

– For etching time typically longer than 90 min; either the methane around the catalyst droplets is in equilibrium with the carbon at the catalyst surface, or there is no hydrogen anymore near the catalyst, and consequently the etching process is stopped.

The etching depth is therefore limited by gas in- and out-diffusion inside the nanopores. In order to justify this hypothesis, a diamond sample was annealed in 60 Torr hydrogen at 800 °C with 0.5% methane. No etching was observed after 60 min of process (Fig. 8a).

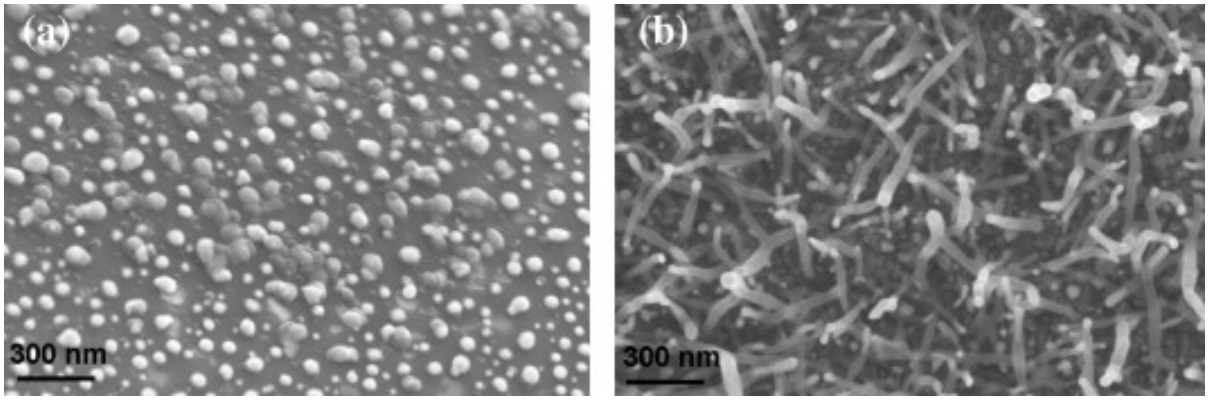

Fig. 8. SEM images of **(a)** (1 0 0) surface of polycrystalline diamond after 60 min annealing in 60 Torr H_2 and 0.5% CH_4 environment showing the compensation of etching by CH_4 molecules, and **(b)** nanocrystalline diamond after 6 h annealing in the closed chamber under 60 Torr H_2 demonstrating the growth of CNTs due to the accumulation of carbon atoms on the catalyst; both samples were processed with 3 nm Ni at 800 °C.

In fact, the methane concentration was high enough to stop the carbon desorption from the catalyst, preventing any etching. Interestingly, the increase in carbon concentration around the catalyst could lead, in some particular conditions, to the reverse process: the growth of CNTs. It was the case, for example, for a nanocrystalline diamond sample annealed in the closed chamber for 6 h with 3 nm Ni layers at 800 °C under 60 Torr hydrogen. The nanotubes (Fig. 8b) clearly grew after a long etching step, the catalyst being located deep inside the microcrystal. The growth mechanism of CNTs on diamond with Ni nanoparticles as catalyst could be found in Ref. [36].

Similarly, a process performed in vacuum does not lead to any etching [17] showing the importance of both hydrogen in-diffusion and methane out-diffusion in the process.

3.4. Model for etching diamond with Ni

After the formation of catalyst droplets by dewetting, five important steps of the process have been identified based on the above investigations, as shown schematically in Fig. 9:

1. Diffusion of molecular hydrogen from the chamber to the surface of the catalyst.
2. Molecular hydrogen is catalytically dissociated into atomic hydrogen by nickel.
3. Carbon atoms from the diamond surface can be removed through two different ways:

a. a.The carbon atoms dissolve in the nickel droplet and then diffuse to the metal–gas interface where they react with hydrogen atoms forming methane.
b. b.Hydrogen atoms diffuse within the catalyst to reach the diamond–metal interface, then remove carbon in the form of methane.

4. Desorption of methane from the catalyst.
5. Out-diffusion of methane from the vicinity of the catalyst.

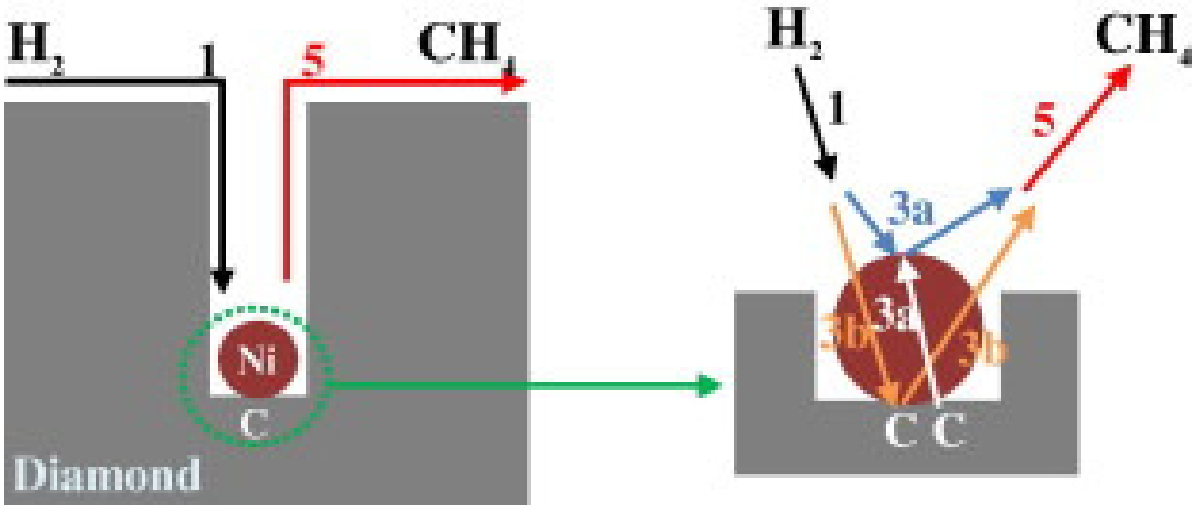

Fig. 9. Schematic representation of the model for etching diamond with Ni; (1) hydrogen diffusion to the catalyst surface, (3a) carbon diffusion from the metal–diamond interface to metal–gas interface and then desorption as methane, (3b) hydrogen diffusion to the diamond–metal interface and carbon desorption as methane and (5) out-diffusion of methane from the vicinity of the catalyst.

For short etching time, when the catalyst is still located close to the diamond surface, step 3 is limiting the etching process. In both cases, 3a and 3b, the reaction is not limited by the diffusion through the catalyst as the etching rate does not decrease with the catalyst thickness. The process is therefore limited by the reaction at the diamond–catalyst interface. The surface study carried out by XPS did not show any evidence of nickel carbide that could have limited the interface reactions.

4. Conclusion

The etching mechanism of diamond using Ni nanoparticles as catalyst was investigated through SEM observation, surface chemistry by XPS and gas composition analysis. A simplified model was proposed to explain the etching mechanism. According to this model, carbon atoms are dissolved into the nickel particle and then transferred to the gas phase as methane with the help of hydrogen. Depending on the kinetics at the diamond surface and the hydrogen in- and methane out-diffusion between the chamber and the etching location, the etching mechanism is either limited by the surface kinetics, as, for example at the beginning of the process, or by the diffusion when the nickel particles are deep inside the diamond layer. This last phenomenon is at the origin of the limitation in depth of the process. However, the understanding of the process, in particular the rate limiting steps allowed us to improve the etching conditions, and nanopores of about 600 nm long were etched into a diamond membrane leading to the fabrication of a porous diamond membrane. This new process opens

many valuable opportunities for the development of diamond technology. Porous diamond membranes are for example key elements for sensors. In addition, controlled surface roughness or well-defined etching pattern will be very useful, and it will boost the development of diamond based applications.

Acknowledgements

The authors would like to thank Vo-Ha for atmospheric pressure experiments. The work was supported by ANR 2010-BLAN-812-03 (VLOC) program.

References

[1] J.J. Kasianowicz, E. Brandin, D. Branton, D.W. Deamer**Characterization of individual polynucleotide molecules using a membrane channel.** Proc Natl Acad Sci USA, 93 (24) (1996), pp. 13770-13773

[2] M. Wanunu, T. Dadosh, V. Ray, J.M. Jin, L. McReynolds, M. Drndic**Rapid electronic detection of probe-specific microRNAs using thin nanopore sensors.** Nat Nanotechnol, 5 (11) (2010), pp. 807-814

[3] S.W. Kowalczyk, A.R. Hall, C. Dekker**Detection of local protein structures along DNA using solid-state nanopores.** Nano Lett, 10 (1) (2010), pp. 324-328

[4] M. van den Hout, A.R. Hall, M.Y. Wu, H.W. Zandbergen, C. Dekker, N.H. Dekker. **Controlling nanopore size, shape and stability.** Nanotechnology, 21 (11) (2010), p. 115304

[5] J. Li, D. Stein, C. McMullan, D. Branton, M.J. Aziz, J.A. Golovchenko. **Ion-beam sculpting at nanometre length scales.** Nature, 412 (6843) (2001), pp. 166-169

[6] T. Mitsui, D. Stein, Y.R. Kim, D. Hoogerheide, J.A. Golovchenko. **Nanoscale volcanoes: accretion of matter at ion-sculpted nanopores.** Phys Rev Lett, 96 (3) (2006), pp. 036102-1-036102-4

[7] M.J. Kim, M. Wanunu, D.C. Bell, A. Meller. **Rapid fabrication of uniformly sized nanopores and nanopore arrays for parallel DNA analysis.** Adv Mater, 18 (23) (2006), pp. 3149-3153

[8] A.J. Storm, J.H. Chen, X.S. Ling, H.W. Zandbergen, C. Dekker**Fabrication of solid-state nanopores with single-nanometre precision.** Nat Mater, 2 (8) (2003), pp. 537-540

[9] J.E. Field**The properties of diamond.** Academic, London (1979) p. 4–22

[10] B.S. El-Dasher, J.J. Gray, J.W. Tringe, J. Biener, A.V. Hamza, C. Wild, *et al.* **Crystallographic anisotropy of wear on a polycrystalline diamond surface.** Appl Phys Lett, 88 (24) (2006), pp. 241915-1-241915-3

[11] O. Auciello, J. Birrell, J.A. Carlisle, J.E. Gerbi, X.C. Xiao, B. Peng, *et al.* **Materials science and fabrication processes for a new MEMS technology based on ultrananocrystalline diamond thin films.** J Phys Condens Matter, 16 (16) (2004), pp. R539-R552

[12] A. Kriele, O.A. Williams, M. Wolfer, D. Brink, W. Muller-Serbert, C.E. Nebel. **Tuneable optical lenses from diamond thin films.** Appl Phys Lett, 95 (3) (2009), pp. 031905-1-031905-3

[13] C.E. Nebel, B. Rezek, D. Shin, H. Uetsuka, N. Yang. **Diamond for bio-sensor applications.** J Phys D, 40 (20) (2007), pp. 6443-6466

[14] B.M. Hausmann, M. Khan, Y. Zhang, T.M. Babinec, K. Martinick, M. McCutcheon, *et al.* **Fabrication of diamond nanowires for quantum information processing applications.** Diamond Relat Mater, 19 (5–6) (2010), pp. 621-629

[15] W. Janssen, E. Gheeraert. **Dry etching of diamond nanowires using self-organized metal droplet masks.** Diamond Relat Mater, 20 (3) (2011), pp. 389-394

[16] W. Janssen, S. Faby, E. Gheeraert. **Bottom-up fabrication of diamond nanowire arrays**

Diamond Relat Mater, 20 (5–6) (2011), pp. 779-781

[17] H.-A. Mehedi, C. Hebert, S. Ruffinatto, D. Eon, F. Omnes, E. Gheeraert. **Formation of oriented nanostructures in diamond using metallic nanoparticles.** Nanotechnology, 23 (45) (2012), p. 455302

[18] S. Konishi, W. Sugimoto, Y. Murakami, Y. Takasu. **Catalytic creation of channels in the surface layers of highly oriented pyrolytic graphite by cobalt nanoparticles.** Carbon, 44 (11) (2006), pp. 2338-2340

[19] Y. Takasu, S. Konishi, W. Sugimoto, Y. Murakami. **Catalytic formation of nanochannels in the surface layers of diamonds by metal nanoparticles.** Electrochem Solid State Lett, 9 (7) (2006), pp. C114-C117

[20] V.G. Ralchenko, T.V. Kononenko, S.M. Pimenov, N.V. Chernenko, E.N. Loubnin, V. YuArmeyev, *et al.* **Catalytic interaction of Fe, Ni and Pt with diamond films: patterning applications.** Diamond Relat Mater, 2 (5–7) (1993), pp. 904-909

[21] S. Barrat, S. Saada, I. Dieguez, E. Bauer-Grosse. **Diamond deposition by chemical vapor deposition process: study of the bias enhanced nucleation step.** J Appl Phys, 84 (4) (1998), pp. 1870-1-1870-11

[22] S. Tanuma, C.J. Powell, D.R. Penn. **Calculations of electron inelastic mean free paths for 31 materials.** Surf Interface Anal, 11 (11) (1988), pp. 577-589

[23] A. Pundt. **Hydrogen in nano-sized metals.** Adv Eng Mater, 6 (1–2) (2004), pp. 11-21

[24] P.C. Yang, W. Liu, R. Schlesser, C.A. Wolden, R.F. Davis, J.T. Prater, *et al.* **Surface melting in the heteroepitaxial nucleation of diamond on Ni.** J Cryst Growth, 187 (1) (1998), pp. 81-88

[25] P. Buffat, J.P. Borel. **Size effect on the melting temperature of gold particles.** Phys Rev A, 13 (6) (1976), pp. 2287-2298

[26] S. Jin, W. Zhu, T. Siegrist, T.H. Tiefel, G.W. Kammlott, J.E. Graebner, *et al.* **Anisotropy in diamond etching with molten cerium.** Appl Phys Lett, 65 (21) (1994), pp. 2675-1-2675-3

[27] V.M. Sonin, A.I. Chepurov, I.I. Fedorov. **The action of iron particles at catalyzed hydrogenation of 1 0 0 and 1 1 0 faces of synthetic diamond.** Diamond Relat Mater, 12 (9) (2003), pp. 1559-1562

[28] S. Konishi, T. Ohashi, W. Sugimoto, Y. Takasu. **Effect of crystal plane on the catalytic etching behavior of diamond crystallites by cobalt nanoparticles.** Chem Lett, 35 (11) (2006), pp. 1216-1217

[29] W. Smirnov, J.J. Hees, D. Brink,W. Muller-Sebert, A. Kriele, O.A. Williams, *et al.***Anisotropic etching of diamond by molten Ni particles.** Appl Phys Lett, 97 (7) (2010), pp. 073117-1-073117-3

[30] J.C. Arnault, S. Saada, S. Delclos, L. Intiso, N. Tranchant, R. Polini, *et al.* **In situ study of the initial stages of diamond deposition on 3C–SiC (1 0 0) surfaces: towards the mechanisms of diamond nucleation.** Diamond Relat Mater, 16 (4–7) (2007), pp. 690-694

[31] M.C. Biesinger, B.P. Payne, L.W.M. Lau, A. Gerson. **Smart RStC. X-ray photoelectron spectroscopic chemical state quantification of mixed nickel metal oxide and hydroxide systems.** Surf Interface Anal, 41 (4) (2009), pp. 324-332

[32] S. Rey, J. Hommet, G. Schmerber, F. Normand**. Surface transformations of carbon (graphene, graphite, diamond, carbide), deposited on polycrystalline nickel by hot filaments chemical vapour deposition.** Thin Solid Films, 519 (14) (2011), pp. 4426-4428

[33] A. Wiltner, C. Linsmeier. **Formation of endothermic carbides on iron and nickel.** Phys Status Solidi A, 201 (5) (2004), pp. 881-887

[34] J.C. Arnault, S. Saada, S. Delclos, L. Intiso, L. Rocha, R. Polini, *et al.* **Surface science contribution to the BEN control on Si (1 0 0) and 3C–SiC (1 0 0): towards ultra thin nanocrystalline diamond films.** Chem Vap Deposition, 14 (7–8) (2008), pp. 187-195

[35] Y. Tamai, H. Watanabe, A. Tomita. **Catalytic gasification of carbon with steam, carbon dioxide and hydrogen.** Carbon, 15 (2) (1977), pp. 103-106

[36] N. Tumilty, L. Kasharina, T. Prokhoda, B. Sinelnikov, R.B. Jackman. **Synthesis of carbon nanotubes on single crystal diamond.** Carbon, 48 (11) (2010), pp. 3027-3032